Supporting Information for

Energy Renormalization Method for the Coarse-Graining of Polymer Viscoelasticity

Jake Song, David D. Hsu, Kenneth R. Shull, Frederick R. Phelan Jr,

Jack F. Douglas, Wenjie Xia*, Sinan Keten*

*Corresponding Authors: wenjie.xia@nist.gov, s-keten@northwestern.edu

Contents

1. Molecular dynamics simulation methods

All MD simulations of PB and PS are carried out using the LAMMPS package.[1] Atomistic models of PB and PS with chain length $N = 10$ are generated using Materials Studio,[2] and comprise of 40 400 atoms and 40 250 atoms respectively. $N = 10$ is chosen for this work primarily due to computational limits – larger chain lengths will require unfeasibly long simulation times to relax properly for the atomistic models. CG models of PB and PS are generated with the same chain lengths, and both comprise of 10 000 CG atoms. The time steps Δt are 10 fs for PB, and 4 fs for PS, respectively, which are chosen based on their bonded vibrational frequency. The CG-PB model is able to handle larger time steps due to its softer bond potential (Figure S2). The systems are prepared by equilibrating in the bulk state, which begins with an energy minimization step via the conjugate gradient algorithm.[3] Following this, the systems undergo annealing cycles above and below the glass transition temperature T_g (between 75 K and 600 K for PB, and 210 K and 750 K for PS) and pressure cycles (between 1 bar and 1000 bar for both systems) in the NPT (i.e., constant number of beads, pressure and temperature) ensemble, and then equilibrated for 2 ns at 600 K and 750 K for PB and PS respectively.

2. Bonded potentials for CG-PB model

To generate effective bond, angle, and dihedral potentials for the CG-PB model based on the force centers identified in the main text, we employ the inverse Boltzmann method (IBM).[4] This procedure involves obtaining the bonded probability distributions of the atomistic PB in the melt state ($T = 400$ K) following the equilibration procedure outlined in Section S1, and inverting the probability distributions via the IBM:

$$U_{bond}(l) = \frac{1}{N}\sum_{i=1}^{N}\left[-k_{\mathrm{B}}T\ln\left(\frac{P_i(l)}{l^2}\right)\right] \tag{S1}$$

$$U_{angle}(\theta) = \frac{1}{N}\sum_{i=1}^{N}\left[-k_{\mathrm{B}}T\ln\left(\frac{P_i(\theta)}{\sin\theta}\right)\right] \tag{S2}$$

$$U_{dihed}(\phi) = \frac{1}{N}\sum_{i=1}^{N}\left[-k_{\mathrm{B}}T\ln\left(P_i(\phi)\right)\right] \tag{S3}$$

where k_{B} is the Boltzmann constant, T is the temperature, P_i is the probability distribution functions for bond length l, angle θ and dihedral angle ϕ. Direct implementation of the atomistically derived Boltzmann potential estimate is typically not perfect, and thus the CG potentials are optimized iteratively to create a good match with atomistic target distributions. The derived CG potentials can be captured analytically, or with a tabulated spline. The former strategy is employed for the CG-PS, and the analytical forms of the potentials can be found in Table S1. More detail on the derivation of the CG-PS potentials can be found in the original publication.[5] The latter strategy is employed for the CG-PB. The resulting probability densities and potentials for PB are shown in Figure S1.

Table S1: Functional form of force field and bonded potential parameters for CG-PS.

Interaction	Potential form	Parameters
A-A Bond Length	$U_{bondAA}(l)=k(l-l_0)^2$	k = 80.69 kcal/mol·Å^2 l_0 = 2.568 Å
A-B Bond Length	$U_{bondAB}(l)=k(l-l_0)^2$	k = 224.6 kcal/mol·Å^2 l_0 = 2.871 Å
A-A-A Angle	$U_{angleAAA}(\theta)=-k_bT\ln\left[a_1\exp-\left(\frac{\theta-\theta_1}{b_1}\right)^2+a_2\exp-\left(\frac{\theta-\theta_2}{b_2}\right)^2+a_3\exp-\left(\frac{\theta-\theta_3}{b_3}\right)^2\right]$	a_1 = 2.277e-1 a_2 = 5.588e-1 a_3 = -5.497e-1 b_1 = 10.76° b_2 = 19.27° b_3 = 18.78° θ_1 = 177.1° θ_2 = 148.8° θ_3 = 148.5°
A-A-B Angle	$U_{angleAAB}(\theta)=-k_bT\ln\left[a_1\exp-\left(\frac{\theta-\theta_1}{b_1}\right)^2+a_2\exp-\left(\frac{\theta-\theta_2}{b_2}\right)^2+a_3\exp-\left(\frac{\theta-\theta_3}{b_3}\right)^2\right]$	a_1 = 1.451e-1 a_2 = 1.767e-2 a_3 = 3.199e-2 b_1 = 6.762° b_2 = 9.745° b_3 = 11.01° θ_1 = 141.5° θ_2 = 93.22° θ_3 = 134.7°
A-A-A-A Dihedral Angle	$U_{dihedralAAAA}(\phi)=A\cos(\phi)$	A (atactic) = 0.5 (kcal/mol)
B-A-A-B Dihedral Angle	$U_{dihedralBAAB}(\phi)=\sum_{k=1}^{5}A_k\cos^{k-1}(\phi)$	*meso* A_1 = 4.236 (kcal/mol) A_2 = -1.274 (kcal/mol) A_3 = 0.5337 (kcal/mol) A_4 = -0.8179 (kcal/mol) A_5 = -0.4622 (kcal/mol) *racemo* A_1 = 3.762 (kcal/mol) A_2 = 0.3631 (kcal/mol) A_3 = 2.128 (kcal/mol) A_4 = -0.9691 (kcal/mol) A_5 = -1.880 (kcal/mol)
Non-bonded	$U_{nonbond}=4\varepsilon(T)\left[\left(\frac{\sigma(T)}{r}\right)^{12}-\left(\frac{\sigma(T)}{r}\right)^{6}\right]+S_{LJ}(r)$	$\varepsilon_{AA}=\alpha(T)\times0.136$ (kcal/mol) $\sigma_{AA}=\beta(T)\times4.60$ (Å) $\varepsilon_{BB}=\alpha(T)\times0.174$ (kcal/mol) $\sigma_{BB}=\beta(T)\times5.06$ (Å)

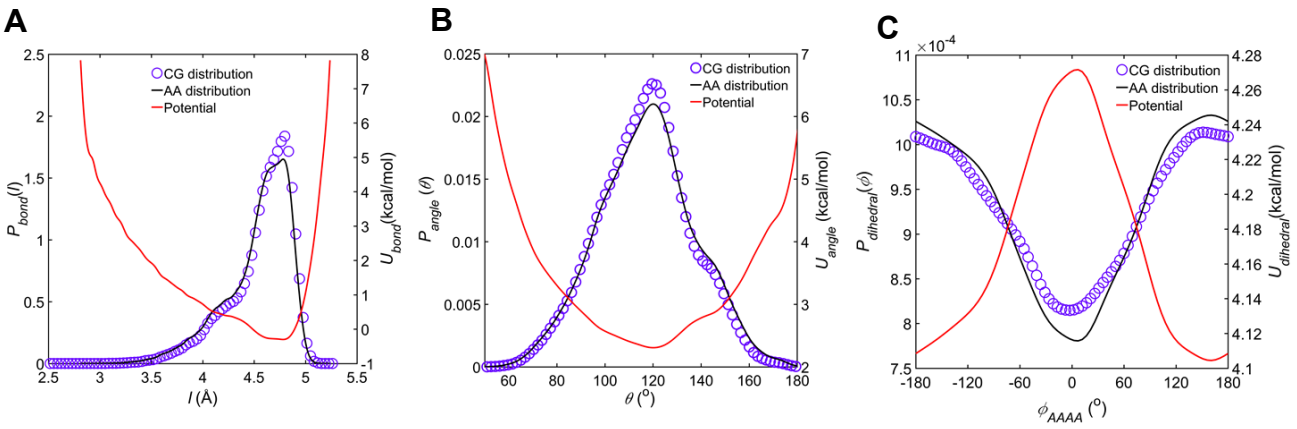

Figure S1. (A) Bond, (B) angle, and (C) dihedral probability distributions and potentials for AA and CG 1,4-*cis* polybutadiene, obtained via the IBM. The probability distributions are based on the force centers identified in Figure 1 of the main manuscript. The tabulated forms of the potentials can be found in the attached data.

We note that the bond potentials derived from IBM provides insight into the degree of coarse-graining λ in CG models as it represents the distance between each CG bead. The steepness of the harmonic function that can be fitted on the potential determines how high of a vibrational frequency the CG model can tolerate, and how large the Δt can be. Accordingly, the bond potentials provide direct information on the capacity of the CG model to tolerate high-frequency dynamics. Figure S2 shows the comparison between CG-PB and CG-PS, and as discussed in the main text, the PB model has a far larger bond length and a broader potential. This may explain why the CG-PB model is less able to capture high frequency viscoelastic properties of the atomistic PB model.

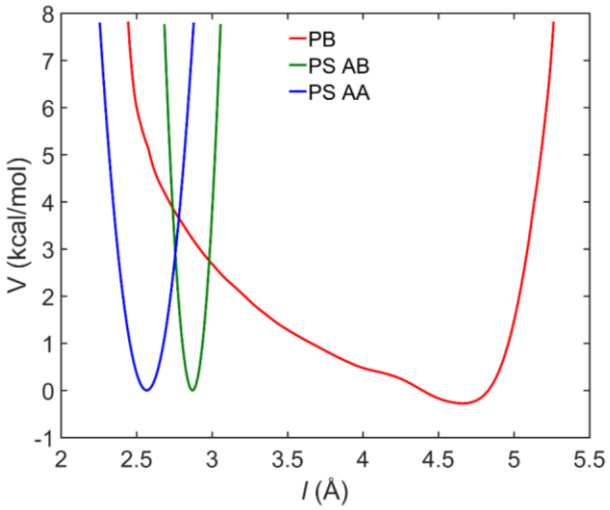

Figure S2. Comparison of bonded potentials of the CG-PB and CG-PS. For the CG-PS, the bonds "AB" and "AA" are defined as the bonds between the backbone and side-group CG beads and between the backbone and backbone CG beads, respectively.

3. Non-bonded potentials for CG models

For both CG PB and PS systems, we adopt the GROMACS style 12-6 Lennard-Jones potential:[6]

$$U_{nonbond} = 4\varepsilon\left[\left(\frac{\sigma}{r}\right)^{12} - \left(\frac{\sigma}{r}\right)^{6}\right] + S_{LJ}(r) \qquad r < r_{outer} \tag{S4}$$

$$S_{LJ}(r) = \frac{E}{3}(r - r_{inner})^3 + \frac{F}{4}(r - r_{inner})^4 + H \qquad r_{inner} < r < r_{outer} \tag{S5}$$

where σ is the length at which $U_{nonbond}$ is zero in nm, and ε is the depth of the potential well in kcal/mol. The polynomial term $S_{LJ}(r)$ is implemented to ensure a smooth transition to zero energy and force from r_{inner} = 1.2 nm to r_{outer} = 1.5 nm. E, F and H are constants.

Unlike the 1-bead CG-PB which requires single values for σ and ε, the 2-bead CG-PS requires three values for σ and ε: σ_{AA} and ε_{AA} for backbone-backbone (AA) interactions, σ_{BB} and ε_{BB} for sidechain-sidechain (BB) interactions, and σ_{AB} and ε_{AB} for backbone-sidechain (AB) interactions. σ_{AB} and ε_{AB} are taken as the arithmetic ($\sigma_{AB} = \frac{1}{2}(\sigma_{AA} + \sigma_{BB})$) and geometric averages ($\varepsilon_{AB} = \sqrt{\varepsilon_{AA}\varepsilon_{BB}}$) of the *AA* and *BB* terms, respectively. To eliminate the added degrees of freedom for PS, we previously adopted temperature scaling factors $\beta(T)$ and $\alpha(T)$ for σ and ε, respectively, while keeping the ratios of $\frac{\sigma_{AA}}{\sigma_{BB}}$ and $\frac{\varepsilon_{AA}}{\varepsilon_{BB}}$ consistent with those obtained from the atomistic radial distribution function of the corresponding CG force centers.[7] As noted in the main text, $\varepsilon(T, f) = \alpha(T, f)/\varepsilon_A$. The values for ε_A are 0.7866 kcal/mol for the CG-PB, and 0.4383 kcal/mol and 0.5608 kcal/mol for the backbone and side-group terms for CG-PS, respectively.

4. Deriving energy renormalization function $\alpha(T)$ for CG-PB

As discussed in the main publication, we make a distinction between temperature-dependent non-bonded potentials derived from EMD and NEMD simulations. NEMD simulations fundamentally sample different potential energy landscapes from EMD due to the perturbations in entropy and CG potentials that are derived from EMD during flow.[8] It also exhibits rate-dependent GF dynamics, in addition to the expected temperature-dependence of GF dynamics. The main work deals exclusively with LJ potentials derived for NEMD properties, but frequently refers to the EMD potentials as it represented the starting point for us to devise the *rate and temperature transferable coarse graining strategy*. It also provides the starting point for the length parameter σ to keep constant while we vary the cohesive interaction parameter ε. We carry out the EMD based $\alpha(T)$ parameterization on the CG-PB. This procedure has been performed for the CG-PS and the method as well as the functional form is detailed in our prior work.[7] Here, we briefly outline the method for calculating the different dynamic properties – high-frequency shear modulus G, segmental relaxation time τ, and self-diffusion coefficient D – to show how we reproduced this strategy for CG-PB.

For the calculation of D_{self}, we calculate the MSD of the center of mass of polymer chains via the Einstein relation of the form:

$$D_{self} = \lim_{t\to\infty} \frac{1}{6t} \left\langle \left| r_{CM}(t) - r_{CM}(0) \right|^2 \right\rangle \tag{S6}$$

where $r_{CM}(t)$ is the position of the center of mass of each chain at time t. We then capture D using a commonly employed Arrhenius relation of the form:

$$D_{self} = D_0 \exp\left(-\frac{\Delta H_a}{k_B T} \right) \tag{S7}$$

where D_0 is a pre-factor associated with activation entropy ΔS_a and ΔH_a is the activation energy of diffusion. Our method involves matching the D_{self} and ΔH_a of AA model using different ε of the CG model, which should be constant for temperature ranges above the Arrrhenius temperature T_A. Indeed, as shown in Figure S3A, the ε data points derived from diffusivity calculations are almost temperature invariant at high temperatures, and becomes temperature variant as the system is cooled.

The segmental relaxation time τ is calculated by the second Legendre order parameter $P_2(t)$:

$$P_2(t) = \frac{3}{2}\left\langle \cos^2 \theta(t) \right\rangle - \frac{1}{2} \tag{S8}$$

where $\theta(t)$ is the angle of a vector under consideration at time t relative to its position at t = 0. The bond vector is parallel to the backbone of the CG polymer chain, and is chosen so that the AA and CG vectors are the same. This means that the CG vectors are between consecutive backbone beads, and the AA vectors are chosen accordingly to sample equivalent length-scales. Since there are 4 backbone C atoms in a CG-PB bead and 2 backbone C atoms in CG-PS bead, the AA-PB vector would be between the 1st and the 5th backbone C atom and the AA-PS vector would be between the 1st and the 3rd backbone C atom, *etc*. We then fit $P_2(t)$ with a stretched exponential function:

$$P_2(t) = \exp\left[-\left(\frac{t}{\tau_{KWW}} \right)^{\beta^{KWW}} \right] \tag{S9}$$

where τ_{KWW} is the Kohlrausch-Williams-Watts (KWW) relaxation, and β^{KWW} is the stretch exponent, which describes the breadth of the relaxation times. τ can be determined as the integral of the KWW curves with the expression: $\tau = \left(\frac{\tau_{KWW}}{\beta^{KWW}}\right) \Gamma\left(\frac{1}{\beta^{KWW}}\right)$, where Γ is the gamma function.

Figure S3B shows the temperature-dependent τ values for AA-PB and AA-PS obtained from the above method, fitted using the Vogel-Fulcher-Tamman (VFT) function of the form $\tau(T) = \tau_0 \exp\left(\frac{DT_0}{T-T_0}\right)$. The fitted VFT parameters for AA-PB and AA-PS are referenced throughout the main text, and are listed in Table S2. By matching AA τ values for PB shown in Figure S3B, we obtain ε values for the CG model shown by the circle symbols in Figure S3A. It is evident that in this GF regime, temperature-dependent ε parameterization is required to match AA dynamics. We thus observe an onset of a sigmoidal trend.

The shear modulus G is calculated by simple shear simulations at a constant rate of 0.5 ns^{-1}, from which the shear modulus G can be obtained from the linear slopes in the elastic regime (~ 2 % strain). G at such high frequencies can be considered an EMD property, as they yield information about the structural relaxation of the polymer system.[9] The stress component in the shear deformation is calculated based on the atomic virial stress tensor:[10]

$$\sigma_{xy} = -\frac{1}{V}\left[\sum_{A}^{n} m_A (v_A)_x (v_A)_y + \sum_{A>B}^{n} \frac{\partial U}{\partial r_{AB}} \frac{(r_{AB})_x (r_{AB})_y}{r_{AB}}\right] \quad \text{(S10)}$$

where V is the volume of the system, n is the total number of CG beads, r_{AB} is the distance between bead pair A and B, U is the total energy of the system, and m_A and v_A denote the mass and velocity of nth bead, respectively. As shown in Figure S3A, the ε values obtained from simple shear eventually plateaus at the complete glass state, which also agrees with our findings for CG-PS.[7] Notably however, the magnitude of the sigmoidal increase in ε is larger than those reported for CG-PS, the reasons for which we discuss in the main text.

For parameterizing σ, a parameter which has governing effect on the density of the material, we find that it does not interact strongly with the polymer's self-diffusion. This allows us to capture ε

in the Arrhenius limit first, tune σ to match AA densities in the Arrhenius regime, and extrapolate a rough parameterization of $\sigma(T)$. We then iterate this procedure for $\sigma(T)$ after completing the full parameterization of $\varepsilon(T)$. For CG-PS, we found that it can be captured by a relatively flat linear function. For CG-PB, we actually find that it is almost temperature independent. The density sweeps performed to obtain $\sigma(T)$ after calibrating $\varepsilon(T)$ are shown in Figure S3B. The functional form of $\varepsilon(T)$ and $\sigma(T)$ for CG-PB and CG-PS derived from EMD are reported in Table S2, represented in $\alpha(T)$ and $\beta(T)$ respectively to stay consistent with the CG-PS model which requires such a pre-factor as it is a two-bead-per-monomer CG model.

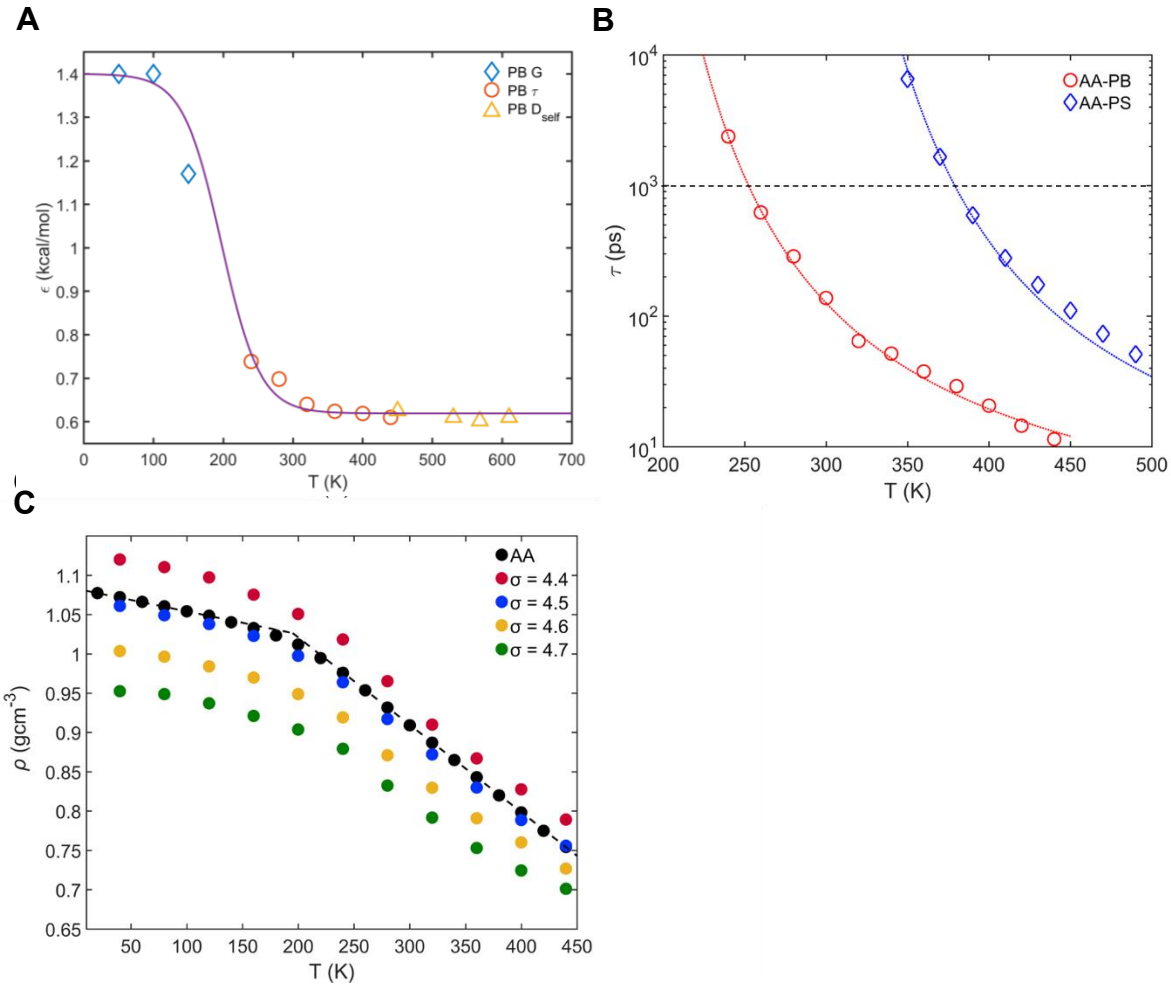

Figure S3. (A) Temperature dependent cohesive strength parameter $\varepsilon(T)$ obtained for CG-PB by matching self-diffusion coefficient D_{self}, the segmental relaxation time τ and the shear modulus G of the AA model spanning over different temperature regimes (i.e., Arrhenius, glass-forming, and glassy regimes). (B) Segmental relaxation time τ as functions of temperature for AA-PB and AA-PS. The dotted lines illustrate VFT fits of the relaxation data, with τ_0 defined to be $\tau_0 = 1$ ps. The dashed black line illustrates the point when $\tau = 1$ ns, i.e. when the system falls out of equilibrium due to vitrification. The VFT fits of AA-PB and AA-PS cross this regime at $T \approx 253$ K and $T \approx 382$ K respectively. (C) Density sweeps as a function of temperature for AA (black symbol) and CG (colored symbols) with varying σ parameters from 4.4 to 4.7 angstroms. Dashed lines on the AA data show a bilinear trend, with the intersection denoting the volumetric T_g. From this figure, σ is identified to be temperature independent, at $\sigma = 4.5$ Å.

Table S2. Functional forms of CG renormalization factors and the VFT fit parameters for the AA models of PB and PS in EMD.

Polybutadiene	Function	Parameters
$\alpha(T)$	$\alpha(T) = \frac{\alpha_A - \alpha_g}{1+\exp\left[-k(T-T_T)\right]} + \alpha_g$	$\alpha_A = 0.6226$ $\alpha_g = 1.40$ $k = 0.03723\ \mathrm{K}^{-1}$ $T_T = 197.5$ K
$\beta(T)$	$\beta(T) = 4.48$	N/A
$\tau(T)$	$\tau(T) = \tau_0 \exp\left(\frac{DT_0}{T-T_0}\right)$	$\tau_0 = 1$ ps $D = 5.44$ $T_0 = 141.2$ K
Polystyrene	Function	Parameters
$\alpha(T)$	$\alpha(T) = \frac{\alpha_A - \alpha_g}{1+\exp\left[-k(T-T_T)\right]} + \alpha_g$	$\alpha_A = 2.33$ $\alpha_g = 3.60$ $k = 0.0185\ \mathrm{K}^{-1}$ $T_T = 475.2$ K
$\beta(T)$	$aT + b$	$a = 1.718\times 10^{-4}\ \mathrm{K}^{-1}$ b =0.9905
$\tau(T)$	$\tau(T) = \tau_0 \exp\left(\frac{DT_0}{T-T_0}\right)$	$\tau_0 = 1$ ps $D = 3.48$ $T_0 = 252.0$ K

5. Calculation of linear viscoelastic properties

Here, we aim to provide more detail on how viscoelastic properties are calculated via NEMD. As discussed in the main text, the viscoelastic properties of the PB and PS systems after equilibration are studied by imposing constant-rate SAOS. This is done under the NVT ensemble, using the SLLOD algorithm which is used to study shear flow behavior.[11] SAOS is applied in the x-y direction, as shown in Figure 2A of the main text. This causes a strain $\gamma(t)$ in the form $\gamma(t) = \gamma_0 \sin\omega t$, where γ_0 is the strain amplitude and $\omega = 2\pi f$ is the input frequency. The resulting virial stress can be fitted using a least-square method in the form of $\sigma_{xy}(t) = \sigma_0 \sin(\omega t + \delta)$, where σ_0 is the maximum stress and δ is the phase angle, and are obtained as such from the fitting (Figure 2B). It must be noted that a direct Fourier transform method can also be used to obtain σ_0 and δ,[12] although we found that in our case, since the response we study is linear and ωt is known *a priori*, the least-square method proved to be more accurate. Having said that, the Fourier transform method proves to be quite useful in testing for limit of the linear viscoelastic regime, for instance, finding the maximum temperature or minimum γ_0, after which thermal noise starts to become too significant for an accurate SAOS study. This procedure is used to identify that AA-PS is unable to sample below $f = 3.3 \times 10^9$ Hz.

The assumption that the stress output from the SAOS simulation is a linear viscoelastic response (LVR) cannot be made *a priori*. Above a maximum γ_0 which should be dependent on system size, frequency and temperature, the polymer will deform in a non-linear manner. As such, we perform an amplitude sweep to determine the maximum γ_0 that can be used to probe the polymer's LVR. This is illustrated as the point beyond which G' and G'' ceases to be linear as functions of γ_0. Figure S4 shows amplitude sweeps for the atomistic PB system at 60 K, 180 K, and 300 K, performed at $f = 10^{10}$ Hz. The 60 K result shows the smallest amplitude regime permissible for

LVR, which is approximately $\gamma_0 = 0.03$, and this grows with temperature (and should TTS hold, shrinks with frequency). We thus pick $\gamma_0 = 0.03$ as the amplitude limit for our atomistic simulations as well as CG simulations, as the CG amplitude analysis results indicated that the results are very similar. Our choice of γ_0 is further supported by results from prior NEMD work by Cifre et al.[13] and Tseng et al.[14], who have both shown that γ_0 can be as high as 0.1.

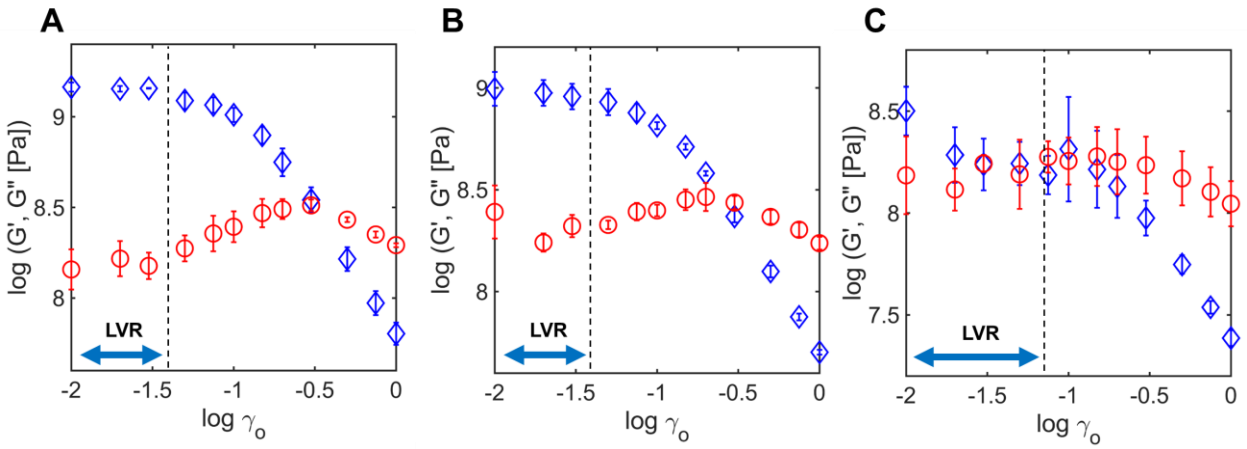

Figure S4. Storage moduli G' and loss moduli $G"$ obtained during oscillation amplitude γ_0 sweeps at (A) T = 60 K, (B) T = 180 K, and (C) T = 300 K performed on AA-PB. The linear viscoelastic regime (LVR), as denoted by the dashed lines in the figures, is defined by the amplitude regime in which the G' and $G"$ readings are roughly independent of the sampling γ_0. Error bars are obtained from three trials.

6. Prediction of viscoelastic properties with the energy renormalization function $\alpha(T, f)$

Figure S5 shows the comparison of $G', G"$ and G^* between the AA and CG models for PB and PS at two different frequencies. Note that PS's low frequency choice of $f = 5 \times 10^9$ Hz is higher than that of PB, since we were unable to resolve a clean viscoelastic reading of PS at lower frequencies, which may be related to the higher temperature of choice and the resulting thermal noise. This is also why Figure 3B in the main text shows a different frequency range for PS compared to PB. Parameterizations are primarily performed on AA G^* at relatively high frequencies, and as a result

the G' and G^* values for AA and CG models at different temperatures and frequencies show good agreement (Figures S5A, S5B, S5E and S5F). However, there is a notable disagreement between AA and CG G'' values for CG-PB below $T \sim 250$ K, which coincides with the onset of the sharply increasing sigmoidal parameterization of α in Figure 3A in the main text, and also coincides with the temperature where segmental relaxation time τ reaches 1 ns. While CG-PS is largely consistent even in this temperature regime, CG-PB's G'' deviates notably from the AA. Despite our efforts to systematically vary non-bonded potentials such as ε and σ (Figure S6), the growing disparity between AA and CG G'' values are still unresolvable. These results suggest that glassy dynamics is indeed a product of local intra-chain relaxation mechanisms, and that the CG-PB model is not able to capture localized glassy dynamics as well as the CG-PS model.

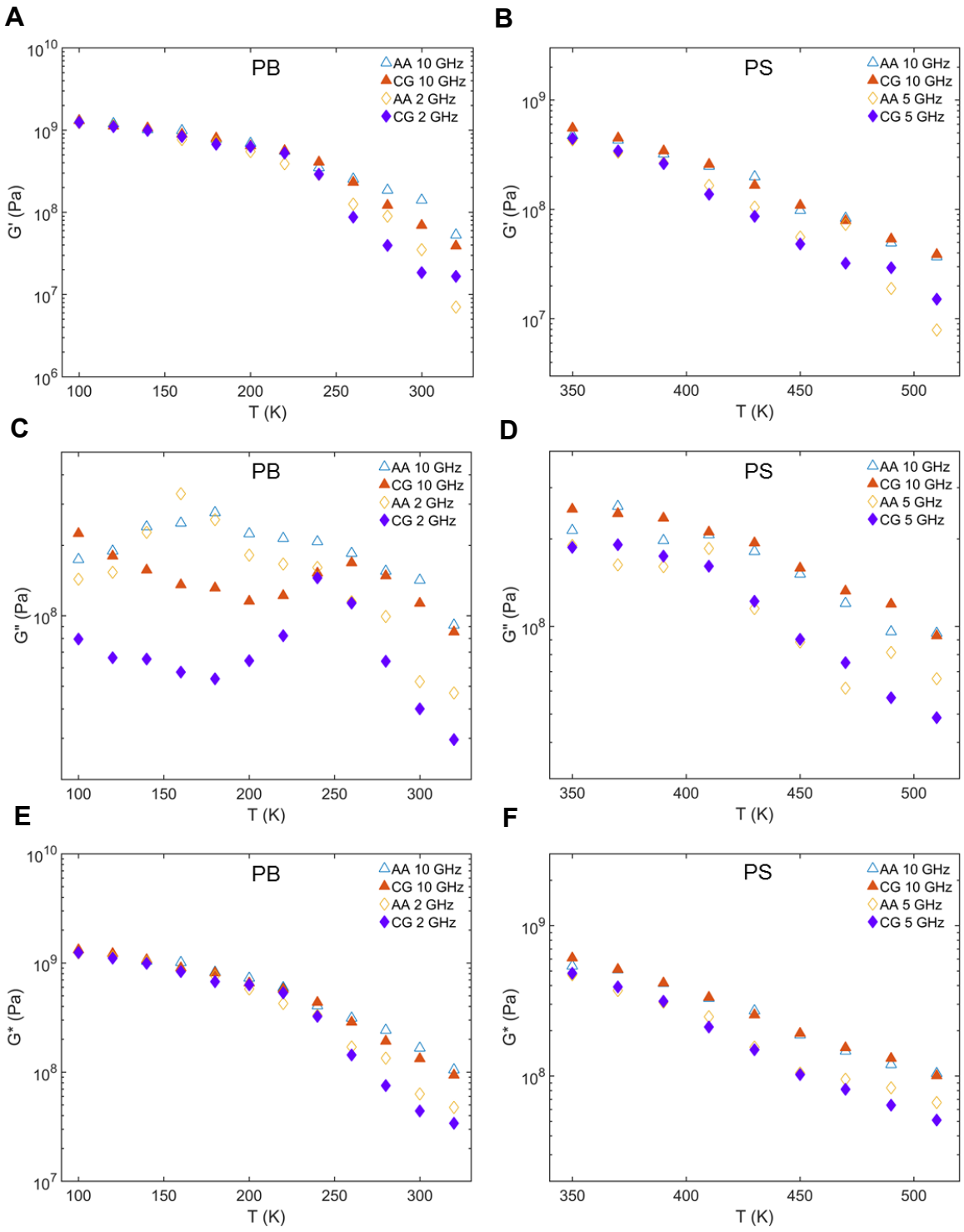

Figure S5. Validation of the ability of CG PB (left column) and PS (right column) models to capture the AA (A, B) storage modulus G' (C, D) loss modulus G", and (E, F) complex modulus G^* at two different frequencies. For the PS model, the lowest frequency is chosen to be 5×10^9 Hz due to the resolution loss experienced by the AA model at 2×10^9 Hz.

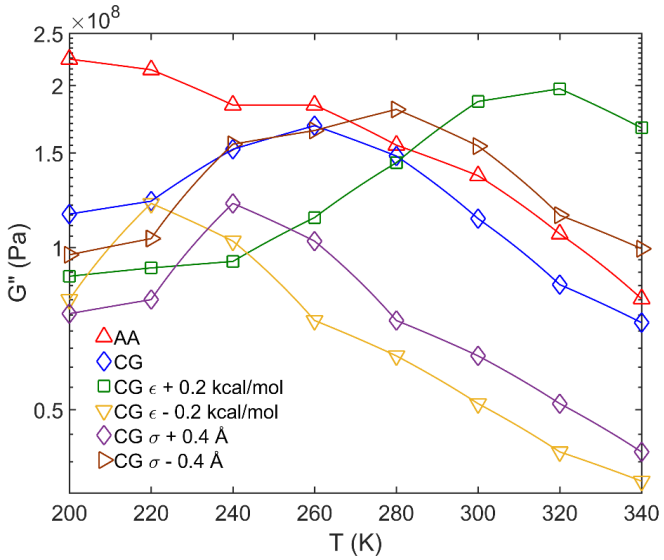

Figure S6. Loss modulus $G^{"}$ plotted against temperature for AA-PB, fully-parameterized CG-PB, and CG-PB models with different iterations of ε and σ, sampled via NEMD at $f = 10^{10}$ Hz. As expected, the cohesive interactions rather than the length parameter dominate the modulus response. However, while tuning ε provides a reasonable match between CG and AA models at higher temperatures ($T > 260$ K), the AA $G^{"}$ values cannot be retained below that temperature by tuning non-bonded interactions alone.

7. Molecular weight effects on the viscoelastic shear modulus

As discussed in the main text, the choice of the number of monomer repeat units per chain N (= 10) in our work is fairly small. Although in theory any N value can be used for our modeling strategy, a small value was chosen to design a computationally feasible project. One concern that must be addressed is whether changing N under the current energy-renormalization scheme forces dramatic changes in the viscoelastic properties. This is a legitimate concern, since the molecular weights used here are in a weight regime where glass-forming dynamics typically experience strong variations with varying N (illustrated by the Flory-Fox relation, for instance). To evaluate this concern in detail, we performed a systematic rheological sweep of the PB model of different molecular weights (Figure S7).

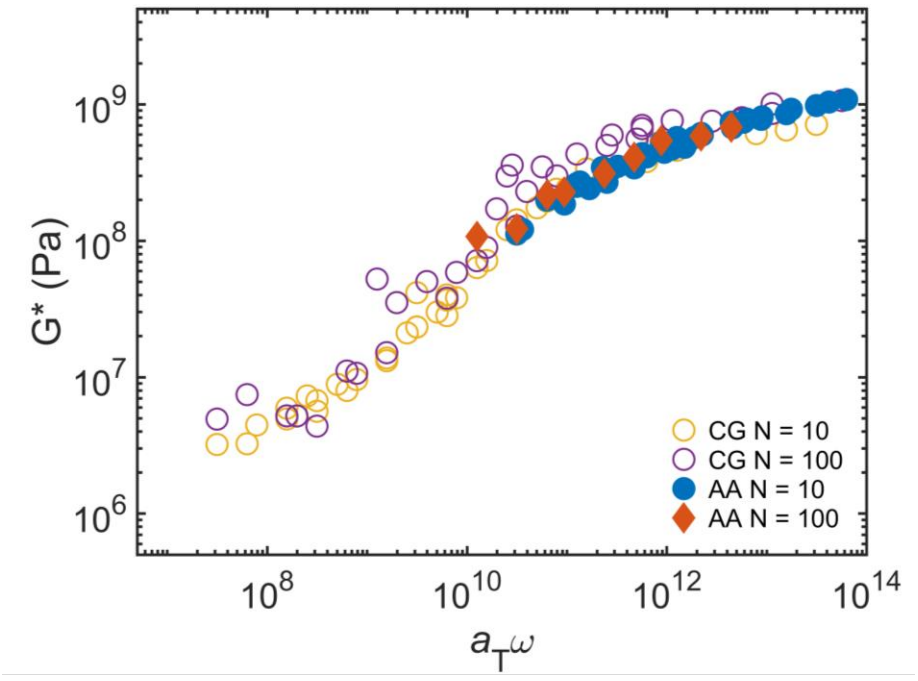

Figure S7. Viscoelastic master curve of the AA and CG models of PB. The horizontal shift factor a_T values for higher N systems were identical to the values obtained for N = 10 (Figure 4B in the main text).

The results show promise for our CG model in capturing *N*-dependent behaviors, in that the higher *N* system shows a rheological response that is slightly stiffened and also shifted to a slightly lower frequency scale. The softening of the system in this regime is directly related to the T_g, and the shifted frequency response agrees with our expectations of *N*-dependent chain end effects on T_g, since the higher *N* system should have a higher T_g (thus requiring *longer* times, or *lower* frequencies to soften).

It is difficult to quantitatively verify the accuracy of the CG predictions based on our ER strategy, as it is difficult to relax the AA model sufficiently for higher *N* systems. As shown in Fig. 1, our AA $N = 100$ model did not show a different viscoelastic response to that of the $N = 10$ model. Ideally, if computational expense was not an issue, our procedure could be repeated for different values of *N* via both atomistic and CG models to validate chain end effects, and verify how (or if at all) α is dependent on *N*. Our expectation is that the same sigmoidal form for the renormalization factor $\alpha(T)$ should apply, but that the cross-over temperature (T_T in Eq. 1 of the current manuscript) might have to be slightly shifted to reflect the shift in T_g with varying *N*. This subject is in fact an important future research topic that we plan to pursue in the future – once a predictive relationship between *N* and $\alpha(T)$ is known, one should be able to use our method without having to perform this correction for each *N* of interest.

8. Parameters for the WLF functions in the main text

Table S3. WLF parameters for the AA and CG systems under consideration. AA-PB, AA-PS and CG-PS values are collapsed when normalized by fragility and Arrhenius temperature, as shown in Figure 4B.

Polybutadiene	$T_{ref}\ (K)$	C_1	C_2
AA	281.0	3.873	211.9
CG	281.0	5.607	228.1
Polystyrene	$T_{ref}\ (K)$	C_1	C_2
AA	549.0	2.398	408.7
CG	549.0	2.874	461.3

9. References

1. Plimpton, S. J., Fast Parallel Algorithms for Short-Range Molecular Dynamics. *J. Comput. Phys.* **1995,** *117*, 1-19.
2. Accelrys, I., Materials Studio. *Accelrys Software Inc* **2010**.
3. Payne, M. C.; Teter, M. P.; Allan, D. C.; Arias, T.; Joannopoulos, J., Iterative Minimization Techniques for Ab Initio Total-Energy Calculations: Molecular Dynamics and Conjugate Gradients. *Rev. Mod. Phys.* **1992,** *64* (4), 1045.
4. Müller-Plathe, F., Coarse-Graining in Polymer Simulation: From the Atomistic to the Mesoscopic Scale and Back. *Chemphyschem* **2002,** *3* (9), 754-769.
5. Hsu, D. D.; Xia, W.; Arturo, S. G.; Keten, S., Thermomechanically Consistent and Temperature Transferable Coarse-Graining of Atactic Polystyrene. *Macromolecules* **2015,** *48* (9), 3057-3068.
6. Lindahl, E.; Hess, B.; van der Spoel, D., Gromacs 3.0: A Package for Molecular Simulation and Trajectory Analysis. *Molecular Modeling Annual* **2001,** *7* (8), 306-317.
7. Xia, W.; Song, J.; Jeong, C.; Hsu, D. D.; Phelan, F. R.; Douglas, J. F.; Keten, S., Energy-Renormalization for Achieving Temperature Transferable Coarse-Graining of Polymer Dynamics. *Macromolecules* **2017,** *50* (21), 8787-8796.
8. Harmandaris, V. A., Quantitative Study of Equilibrium and Non-Equilibrium Polymer Dynamics through Systematic Hierarchical Coarse-Graining Simulations. *Korea-Australia Rheology Journal* **2014,** *26* (1), 15-28.
9. Puosi, F.; Leporini, D., Communication: Correlation of the Instantaneous and the Intermediate-Time Elasticity with the Structural Relaxation in Glassforming Systems. *The Journal of Chemical Physics* **2012,** *136* (4), 041104.
10. Heyes, D. M., Pressure Tensor of Partial-Charge and Point-Dipole Lattices with Bulk and Surface Geometries. *Physical Review B* **1994,** *49* (2), 755-764.
11. Evans, D. J.; Morriss, G., Nonlinear-Response Theory for Steady Planar Couette Flow. *Phys. Rev. A* **1984,** *30* (3), 1528.
12. Lacevic, N. M.; Sader, J. E., Viscoelasticity of Glycerol at Ultra-High Frequencies Investigated Via Molecular Dynamics Simulations. *The Journal of Chemical Physics* **2016,** *144* (5), 054502.
13. Cifre, J. G. H.; Hess, S.; Kröger, M., Linear Viscoelastic Behavior of Unentangled Polymer Melts Via Non-Equilibrium Molecular Dynamics. *Macromol. Theory Simul.* **2004,** *13* (9), 748-753.
14. Tseng, H.-C.; Wu, J.-S.; Chang, R.-Y., Linear Viscoelasticity and Thermorheological Simplicity of N-Hexadecane Fluids under Oscillatory Shear Via Non-Equilibrium Molecular Dynamics Simulations. *PCCP* **2010,** *12* (16), 4051-4065.